EurJIC
European Journal of Inorganic Chemistry

Research Article
doi.org/10.1002/ejic.202500270

Chemistry Europe
European Chemical Societies Publishing

www.eurjic.org

Zinc and Cobalt Coordination Polymers Based on the Redox-Active Linker 4,4′-(Phenazine-5,10-diyl)dibenzoate: Structures and Electrochemical Properties

Dietrich Püschel, Moritz Nau, Nabil Assahub, Thi Hai Yen Beglau, Nils Hufnagel, Dustin Jordan, Tobias Heinen, Till Strothmann, Markus Suta, Rainer F. Winter,* and Christoph Janiak*

The novel coordination polymers $[Zn(PZDB)(DEF)_2]_n$ (Zn-PZDB) and $[Co(HPZDB)_2(DEF)_2]_n$ (Co-HPZDB) (H_2PZDB = 4,4′-(phenazine-5,10-diyl)dibenzoic acid, DEF = *N,N*-diethylformamide) are synthesized solvothermally from the metal nitrate salts and the linear H_2PZDB linker with the redox-active phenazine-5,10-diyl core. Zn–PZDB is composed of zigzag chains with the Zn ion tetrahedrally coordinated by two diethylformamide (DEF) molecules and two carboxyl O-atoms from the bridging $PZDB^{2-}$ linker. The crystal structure of Co-PZDB represents a two-dimensional (2D) coordination grid. The Co^{2+} ion is octahedrally coordinated by two DEF molecules and four carboxyl oxygen atoms of the semi-deprotonated $HPZDB^{-}$ linker molecules. Yellow Zn-PZDB and red Co-PZDB turn green upon air exposure, which is due to linker oxidation, forming the $(H)PZDB^{+}$ radical cation. UV/Vis/NIR spectroelectrochemistry reveals that Me_2PZDB undergoes two reversible one-electron oxidations, producing characteristic absorption bands. Similar spectroscopic changes are observed upon oxidation of Zn-PZDB and Co-HPZDB. Chemical oxidation with $SbCl_5$ yields the same color changes together with electron paramagnetic resonance signals typical of ligand-based radical cations. These findings indicate that the PZDB linker is the primary redox site. Ligand oxidation is followed by disintegration of the coordination polymers.

1. Introduction

The synthesis and design of coordination polymers (CPs) and metal-organic frameworks (MOFs) have gained significant attention in recent years due to their unique architectures and diverse functional properties. CPs are crystalline solids with infinite chains or networks in one, two, or three dimensions, maintained by coordination bonds between metal ions or metal clusters and organic bridging ligands denoted as linkers.[1,2] MOFs are a subclass of CPs with potential porosities, often due to the utilization of spatially elongated linkers.[3,4] These materials have significant potential for various applications in luminescence, biomedicine, gas adsorption, as well as gas storage and separation.[5–10] Organic polycarboxylate anions have been established as widely used linkers for CPs and MOFs. They favor the formation of multinuclear clusters that act as secondary building units (SBUs) with a fixed coordination geometry and connectivity, often rendering them electroneutral by compensating the charge at the metal or cluster cations. The targeted construction of CPs nevertheless warrants a rational design and sensible use of polytopic linkers.[8,11,12]

Redox-active CPs and MOFs enable the investigation of charge transfer mechanisms and applications in chemosensing, electrocatalysis, and optoelectronics. The integration of redox-active ligands or multivalent metal centers facilitates the tuning of electronic, magnetic, and spectroscopic properties. However, challenges such as structural instability during redox cycling necessitate careful design of metal-ligand systems. Advances such as post-synthetic modifications and the incorporation of redox-active guests often serve the purpose of improving stability and functionality. These materials show great potential for technologies such as batteries and catalysis, with ongoing research focused on optimizing CPs and MOFs for enhanced performance and durability.[13–15] Examples for redox-active ligands in coordination polymers and networks are substituted 4,4′-bipyridinium ligands, so-called viologens,[16,17] guanidines,[18,19] and linkers with tetrathiafulvalene (TTF) cores.[20–23]

D. Püschel, N. Assahub, T. H. Y. Beglau, N. Hufnagel, D. Jordan, T. Heinen, T. Strothmann, C. Janiak
Institut für Anorganische Chemie und Strukturchemie
Heinrich-Heine-Universität Düsseldorf
Universitätsstraße 1, D-40225 Düsseldorf, Germany
E-mail: Janiak@uni-duesseldorf.de

M. Nau, R. F. Winter
Fachbereich Chemie
Universität Konstanz
Universitätsstraße 10, D-78457 Konstanz, Germany
E-mail: Rainer.Winter@uni-konstanz.de

M. Suta
Anorganische Photoaktive Materialien
Heinrich-Heine-Universität Düsseldorf
Universitätsstraße 1, D-40225 Düsseldorf, Germany

Supporting information for this article is available on the WWW under https://doi.org/10.1002/ejic.202500270

The use of carboxylate linkers that are also redox-active, such as phenazine-based linkers, for the synthesis of novel CPs and MOFs provides a further opportunity to exploit redox properties. Phenazines feature a dibenzo-anellated pyrazine core and are known for their inherent redox activity. Phenazines are easily reduced to 5,10-dihydrophenazines, which, when combined with further conversions, provide access to a rich variety of dihydrophenazine derivatives (**Scheme 1**).[24] Dihydrophenazines (DHPs), and in particular *N,N′*-substituted diaryl-phenazin-5,10-diyls are electron-rich and form stable radical cations under irradiation, heating, electrolysis, or treatment with a suitable chemical oxidant. Due to their remarkable redox activity and their stable radical cations.[25,26] DHPs exhibit unique optical, electronic, magnetic, and catalytic properties.[27–29] Several diaryl DHPs have been reported as promising photoredox catalysts for visible light-activated atom transfer radical polymerization.[30]

Dihydrophenazine-based organic polymers,[27,31] coordination cages,[32] and MOFs have been investigated as heterogeneous catalysts.[28,33] DHP-based 2D and 3D covalent organic frameworks (COFs) were found as efficient heterogeneous photocatalysts for the radical ring-opening polymerization of vinylcyclopropanes.[31] The UiO-type MOF $[Zr_6(\mu_3\text{-}O)_4(\mu_3\text{-}OH)_4(PZDB)_6]$ was successfully employed as a heterogeneous donor component for enhanced catalytic electron donor acceptor photoactivation.[28] $[Zn_2(PZDB)_2(DABCO)]\cdot 4DMF$ was applied as a heterogeneous catalyst for aza-Diels-Alder reactions (DABCO = 1,4-diazabicyclo[2.2.2]octane).[34] Further, DHP-based coordination cages[35] and porous organic polymers GT-POP-1 (precursor: 4,4′-(phenazine-5,10-diyl)dibenzonitrile), POP1/2 and POP2-Ni (precursor: 5,10-bis(4-vinylphenyl)-5,10-dihydrophenazine) have been studied with respect to their electrochemical properties.[36,37]

In addition to their use as heterogeneous catalysts, dihydrophenazines represent a promising, inexpensive, and environmentally friendly alternative as a cathode material in batteries.[38–40] For instance, molecular DHP derivatives can be embedded in polymers to enhance the electrochemical properties.[41] The lithium salt of $PZDB^{2-}$ (Li_2-PZDB) can be used as a bipolar active material for organic symmetric battery cells, serving both as a cathode and an anode. The dihydrophenazine moiety is cathode-active, while the benzoate moiety is anode-active.[42] Hence, it is of interest to develop new (coordination) polymers based on DHP and investigate their electrochemical properties.

In this work, we present the synthesis and characterization of two new coordination polymers based on the DHP-derived redox-active linker $PZDB^{2-}$.

2. Results and Discussion

The synthesis of the linker acid 4,4′-(phenazine-5,10-diyl)dibenzoic acid (H_2PZDB) is illustrated in Scheme 1. The first step in the synthesis is the reduction of phenazine to DHP. In the second step, the DHP is subjected to a palladium-catalyzed Buchwald–Hartwig coupling with methyl 4-bromobenzoate. The intermediate ester (Me_2PZDB) is subsequently hydrolyzed to give the free dicarboxylic acid H_2PZDB with an overall yield of up to 75%.[42] Its purity and identity were confirmed by ^{1}H NMR, ^{13}C NMR, infrared and high-resolution mass spectrometry, elemental analysis and single-crystal structure analysis (see ESI for details).

The free acid H_2PZDB could be crystallized from DMSO as a DMSO solvate, H_2PZDB·2DMSO as yellow platelets in the triclinic space group $P\bar{1}$ (no. 2). In the crystal structure, the pyrazine centroid coincides with the inversion center, rendering half of the molecule as the crystallographic unique asymmetric unit (**Figure 1**). The annelated benzo and pyrazine rings are nearly coplanar (dihedral angle 0.76(6)°). The dihedral angle between the benzoic acid aryl group and the pyrazine ring is 79.36(7)°, similar to phenazine-5,10-diyl-dibenzonitriles.[43] The intermolecular packing is controlled by C—H···π contacts (see ESI for details).

The reactions of zinc(II) or cobalt(II) nitrate with H_2PZDB under solvothermal conditions in diethylformamide (DEF) resulted in the formation of yellow thin platelet crystals of $[Zn(PZDB)(DEF)_2]_n$ (Zn-PZDB) (Figure S8, Supporting Information), or hexagonal dark red-purple crystals of $[Co(HPZDB)(DEF)_2]_n\cdot DEF$ (Co-HPZDB) (Figure S19, Supporting Information).

Zn-PZDB crystallizes in the monoclinic space group $C2/c$ (no. 15) in a structure determination at 298 K and in the triclinic space group $P\bar{1}$ (no. 2) at 150 K. The room-temperature structure

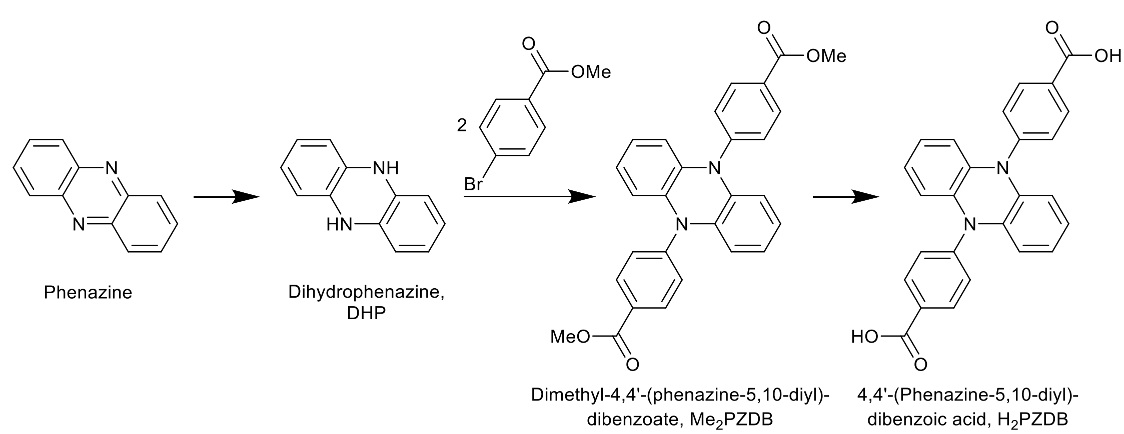

Scheme 1. Synthesis route to the linker 4,4′-(phenazine-5,10-diyl)dibenzoic acid (H_2PZDB).

Research Article
doi.org/10.1002/ejic.202500270

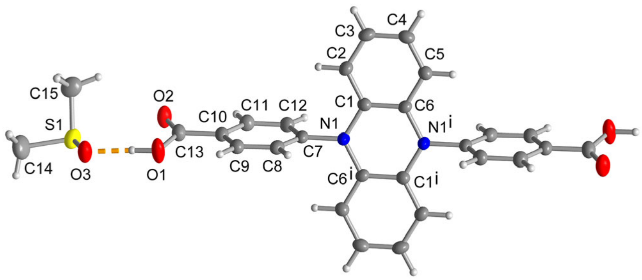

Figure 1. Molecular structure of $H_2PZDB{\cdot}2DMSO$ in the crystal (50% thermal ellipsoids, H atoms with arbitrary radii). Hydrogen bonding interaction (dashed orange line) with O1—H1 = 0.93(3) Å, H1…O3 = 1.65(3) Å, O1…O3 = 2.578(2) Å, O1—H1…O3 = 176°. Symmetry code $i = -x+2,\ -y+1,\ -z+2$.

has a crystallographically unique Zn atom (on a two-fold rotation axis and glide plane), one unique DEF molecule and half a linker (inversion center at the pyrazine centroid) (Figure S12 and S17a, Supporting Information). The lower-symmetry low-temperature structure has two crystallographically different Zn atoms, four DEF ligands and two linkers, none of them on a special position (**Figure 2**, Figure S13 and S17b, Supporting Information). Other than that, the two polymorphic structures from the single-crystal-to-crystal transition are almost identical, with only minor differences in the bond lengths and atomic parameters. The structure of catena-[bis(*N,N*-diethylformamide)-μ-4,4′-(phenazine-5,10-diyl)dibenzoato-κ^2*O,O*″-zinc(II)], Zn-PZDB, is a one-dimensional zigzag chain. A topological analysis (carried out with the program *TopCryst*[44]) assigns the topology **2C1,** which is a very common topology for such zigzag structures.[45] The distance between the Zn(II) ions in a chain is 19.3 Å, with a Zn···Zn···Zn angle of 114°. The tetrahedral coordination environment of Zn is composed of two carboxylate oxygen atoms from two monodentate $PZDB^{2-}$ linkers and two oxygen atoms from two DEF molecules. One-dimensional zigzag chains of Zn(II) or Co(II) ions

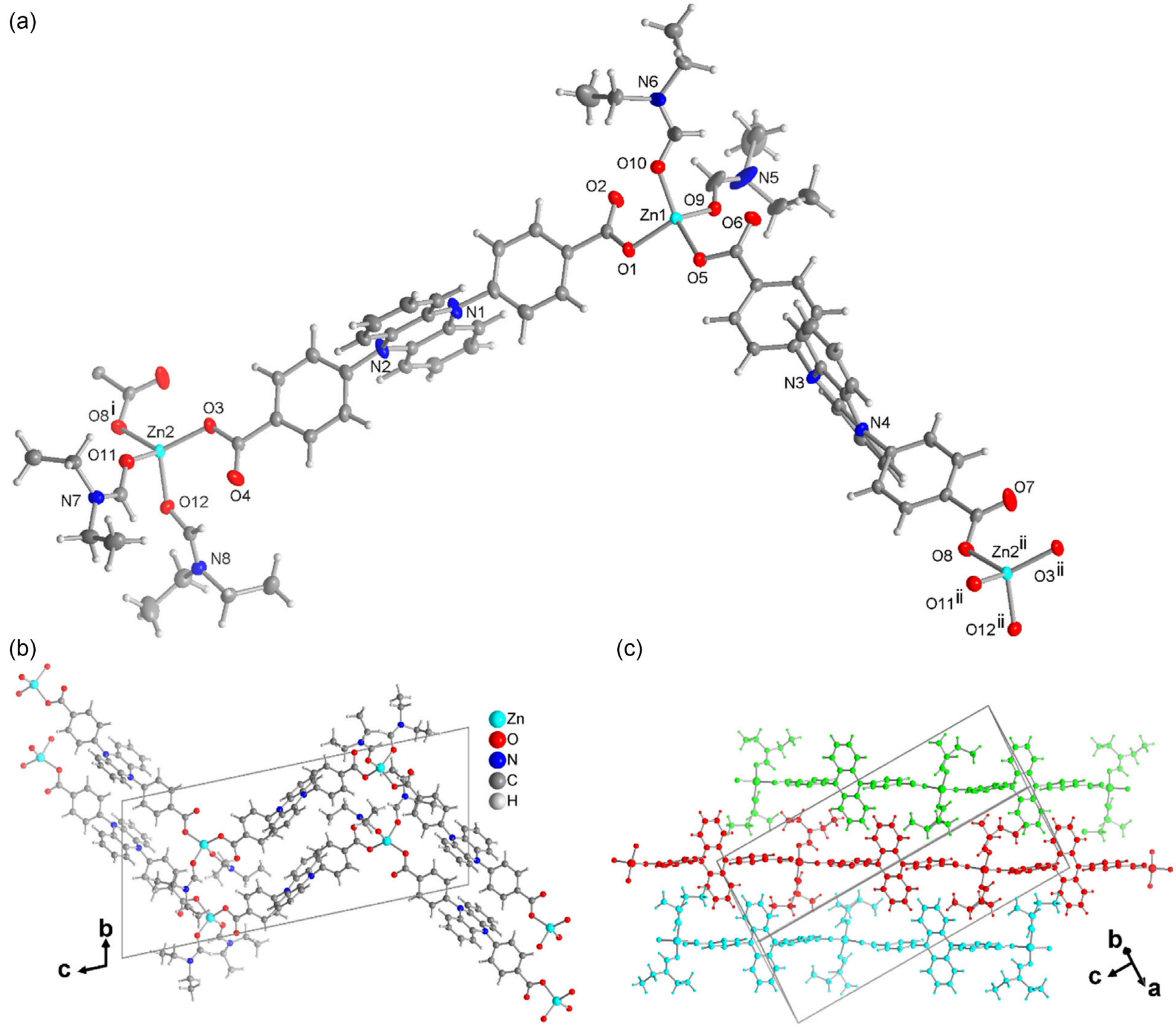

Figure 2. a) Expanded asymmetric unit of Zn-PZDB (150 K structure) with the two symmetry-independent Zn atoms and $PZDP^{2-}$ linkers (50% thermal ellipsoids, H atoms with arbitrary radii). Symmetry transformations: 1) $x-1,\ y+1,\ z+1$; 2) $x+1,\ y-1,\ z-1$. b,c) Chain arrangement in Zn-PZDB. In (c) three different chains are depicted in different colors to help to visualize the "tongue-and-groove" interdigitation motif for the inter-chain packing. See (Figure S13, Supporting Information) for full atom labeling in the asymmetric unit.

Research Article
doi.org/10.1002/ejic.202500270

with carboxylate ligands are frequently observed in dicarboxylate coordination polymers, as exemplified by $[Zn(BDC)(DMP)_2(H_2O)]_n$ and $[Co(BDC)(DMP)_2]_n$ (BDC^{2-} = benzene-1,4-dicarboxyate, terephthalate, DMP = 3,5-dimethylpyrazole) or $[Zn(DHBDC)(PYAOX)_2]_n$ ($DHBDC^{2-}$ = 2,5-dihydroxyterephthalate, PYAOX = pyridine-2-amidoxime).[45,46]

In the low-temperature structure the Zn—O_{carb} bonds range from 1.928(2) to 1.947(2) Å, while the Zn—O_{DEF} bonds are slightly longer, between 1.968(2) and 2.007(2) Å. The O—Zn—O angles lie in between 96.82(7)° and 125.07(7)° (Table S4; see S3, Supporting Information for room-temperature structure). Each $PZDB^{2-}$ linker bridges two zinc ions. The benzoate aryl groups (bzate) and the annelated benzo (bz) groups on the pyrazine (py) ring are slightly *cis*-bent to each other. The angles between the ring centroids (Ct) are Ct_{bzate}-Ct_{py}-Ct_{bzate} = 177° and 172° and Ct_{bz}-Ct_{py}-Ct_{bz} = 175° and 171° for the $PZBD^{2-}$ linkers with N1/N2 and N3/N4, respectively. The dihedral angles between the benzoate aryl groups and the pyrazine ring vary from 82.4(1)° to 88.9(1)°. Adjacent Zn-PZDB chains are arranged parallel to each other. In the room-temperature structure, the chains lie in the {4 0 −4} lattice planes, in the low-temperature structure in the {1 −1 2} planes (Figure S18, Supporting Information).

There are no $\pi\cdots\pi$ interactions between the aromatic rings to organize the inter-chain packing. Instead, the packing of adjacent chains is controlled by a few weak C—H···O_{carb} interactions and by van-der-Waals interactions through the mutual interdigitation, or a "tongue-and-groove" motif of the "tongues" of the diethyl groups from DEF and the annellated benzo groups of the phenazine rings into the "grooves" formed by these alternating "tongues" of the adjacent chains. Evidently, the DEF ligands keep the chains at a certain distance so that no $\pi\cdots\pi$ or C—H···π interactions develop between the aromatic rings. The dense packing of the parallel chains prevents the occlusion of solvent of crystallization.

In view of the important role of the DEF ligands, we crystallized Zn-PZDB also from *N,N*-dimethylformamide (DMF). The structure, which is essentially identical to the one from DEF, is only presented and discussed in the Supporting Information (Section S5, Figure S16 and S17, Supporting Information).

Co-HPZDB crystallizes in the orthorhombic space group *Ccce* (no. 68). The structure is composed of two-dimensional layers with square-lattice (**sql**) topology based on the repeating formula unit $Co(HPZDB)_2(DEF)_2$. Noteworthy, the linker is a mono-deprotonated mono-anion $HPZDP^-$. Two mono-ionic $HPZDP^-$ linkers per formula unit give a charge-balanced formula unit with Co(II). The asymmetric unit of Co-HPZDB contains half a $HPZDB^-$ linker, a Co(II) ion and one molecule of DEF, with two-fold rotations axes passing through the centroid of the pyrazine ring and the Co atom. **Figure 3** shows the extended asymmetric unit with the coordination environment of the Co(II) ion in Co-HPZDB.

The Co(II) ion is sixfold coordinated by four carboxylate and two DEF oxygen atoms in a distorted octahedral geometry. The Co—O(DEF) bond (2.109(6) Å) is slightly longer than the charge-supported Co—O(carboxylate) bond (2.086(3) Å). The O—Co—O angles range from 76.6(2)° to 178.0(2)°. The oxygen atoms of the unique carboxyl group in Co-HPZDB have large

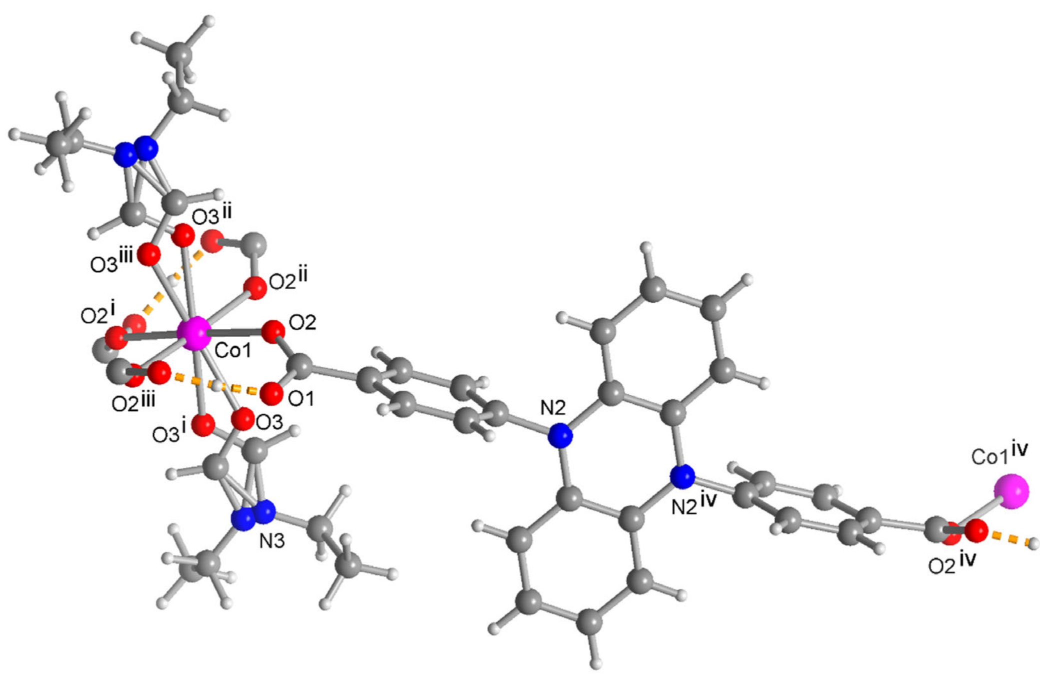

Figure 3. Extended asymmetric unit of Co-HPZDB. For clarity, a ball-and-stick presentation is chosen (see Figure S25, Supporting Information for the thermal ellipsoids). The C_2 axis through the Co atom induces the two positions of the OCHN atoms of DEF with equal occupancy. The half-occupied H atom was arbitrarily placed at a maximum of electron density found at midpoint between the symmetry-related O1 atoms but the actual O—H···O bond will be unsymmetric. Symmetry transformations: 1) $-x+1$, y, $-z+3/2$; 2) x, $-y+3/2$, $-z+3/2$; 3) $-x+1$, $-y+3/2$, z; 4) $-x+1/2$, $-y+1$, z. See (Figure S25, Supporting Information) for full atom labeling in the asymmetric unit.

thermal ellipsoids, which are evidence of a tilt disorder that was also separately refined with two independent A and B oxygen positions (see Figure S26, Supporting Information for further details).

The mono-deprotonated $HPZDP^-$ linkers connect two Co atoms and the non-deprotonated carboxyl group, —COOH forms an H-bond to the *cis*-positioned, deprotonated carboxylate group COO^- around the Co atom. The distance between the two O atoms in the O(—H)···O hydrogen bond is 2.44 Å. Due to the high symmetry in the X-ray structure with only a single unique carboxyl group, the H atom will be seen at both carboxyl groups of the $HPZDP^-$ linker and will, thus, be half-occupied. Because of the additional tilt-disorder of the carboxyl groups (see Figure S26, Supporting Information), this half-occupied H atom could not be located and was arbitrarily placed at a maximum of electron density found at midpoint between the symmetry-related O1 atoms (cf. Figure 3), but the actual O—H···O bond will be unsymmetric. Such an H-bond between a non-deprotonated and deprotonated carboxyl group around a metal center has rarely been observed. A search in the Cambridge structure data base yields only two examples with Co: $[Co_2(dps)_2(5\text{-Br-Hip})_4]_n$ (dps = 4,4′-dipyridylsulfide, 5-Br-H_2ip = 5-bromoisophthalate),[47] and bis[3-(4-carboxyphenoxy)propionato-κO]bis[3-(4-carboxyphenoxy)propionic acid-κ*O*]bis(pyridine-κ*N*)cobalt(II).[48] Further, there is a coordination polymeric Mn network $\{[Mn_3(HBTC)_2(H_2BTC)_2(DMF)_4(H_2O)_2]\cdot 4DMF\}_n$ (H_3BTC = benzene-1,3,5 tricarboxylic acid).[49]

In the C_2-symmetric $HPZDB^-$ linker, the angles between the ring centroids (Ct) are Ct_{bzate}-Ct_{py}-Ct_{bzate} = 173° and Ct_{bz}-Ct_{py}-Ct_{bz} = 179°. The dihedral angle between the benzoic acid aryl group and the pyrazine ring is almost perpendicular (89.4(1)°). The bridging action of four $HPZDB^-$ linkers around cobalt gives rise to a two-dimensional (2D) network with square-lattice (**sql**) topology (**Figure 4**a). The layers in the network lie parallel to the crystallographic *ab* plane. The linkers and their phenazine rings form two planes in each layer (Figure 4b). Parallel networks are arranged in a staggered fashion so that no voids or channels are formed. The distance between the cobalt(II) ions within a layer is 17.7 Å. The Co···Co···Co angles are 61° and 119°, respectively. The distance between the individual layers is 4.9 Å.

Powder X-ray diffraction (PXRD) analyses indicated that as-synthesized Zn-PZDB and Co-HPZDB have a high crystalline phase purity according to the good matches between the experimental and simulated patterns from single-crystal structure data, respectively (**Figure 5**). However, both coordination polymers exhibit a significantly different PXRD pattern after a 24 h exposure to air (Figure S22, Supporting Information). This is accompanied by a change in color from the original yellow in Zn-PZDB and dark red-purple in Co-HPZDB to dark green (Figure S8 and S20, Supporting Information). The observed color change is attributed to the oxidation of the diarylphenazine core. This phenomenon has been previously observed in other dihydrophenazine derivatives.[50,51] The formation of a stable radical cation results in a shift in the charge balance or charge neutrality within the CPs, which contributes to the decomposition of both CPs. Under the employed experimental conditions, the structural disintegration of the coordination polymers upon linker oxidation is irreversible. Neither PXRD nor visual inspection revealed any signs of reassembly or partial structural recovery. The green color of the oxidized material remains unchanged for several weeks and even months under ambient conditions, which suggests that the oxidized phase is stable in the long term. It is also noteworthy that reassembly processes in coordination polymers typically require carefully controlled conditions, such as solvent-mediated recrystallisation or the re-introduction of linkers or metal centres. These conditions were not present in the experimental setup, which further supports the observed irreversibility.

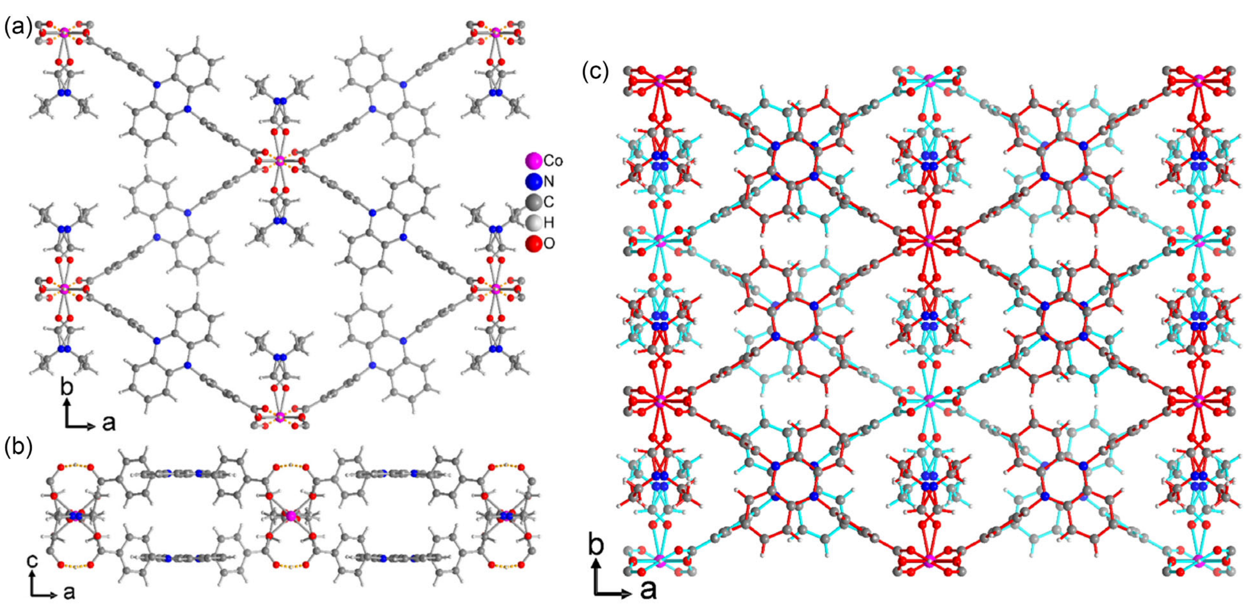

Figure 4. a,b) Section of a single-layer arrangement in Co-HPZDB with (a) top-down view (along the *c* axis), and (b) side view (along *b* axis). In c) the two different layers are depicted in different colors to help to visualize the staggered motif for the inter-layer packing.

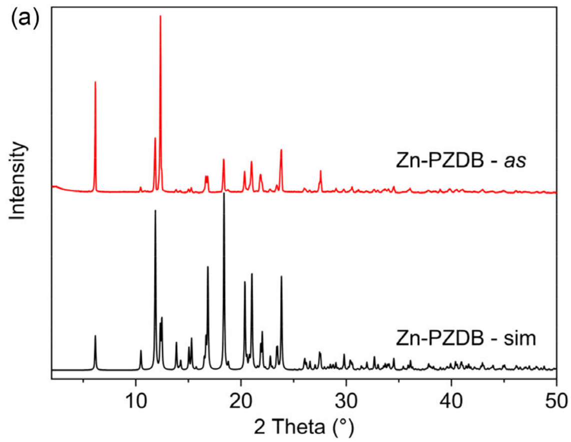

Figure 5. Comparison of the experimental (as = as synthesized) and simulated powder X-ray diffractogram of a) Zn-PZDB (simulation from room-temperature structure), and b) Co-HPZDB. The diffractograms were measured directly after washing and before drying.

Solid-state luminescence/emission spectra were measured at room temperature in order to investigate the photophysical properties. Zn-PZDB exhibits a broad emission with a maximum at 595 nm upon excitation at 400 nm (**Figure 6**a). Additionally, a small shoulder at 804 nm can be resolved. Unlike Zn-PZDB, Co-HPZDB exhibits a markedly red-shifted emission profile, characterized by a weak and broad emission peak with a maximum at 858 nm upon excitation at 450 nm (Figure 6b), which could be related to a localized d^7-d^7 transition of the Co^{2+} ions in an octahedral ligand field. Time-resolved photoluminescence spectra of Zn-PZDB and Co-HPZDB reveal a decay in the nanosecond range as well as a delayed component in the μs range with lower amplitudes (see Figure S28, S29, and S31, Supporting Information). In agreement to various dihydrophenazine derivatives,[24,43] both coordination polymers also show both prompt and delayed fluorescence at room temperature indicating that also ligand-centered luminescence can be detected.

For Zn-PZDB, we attribute the observed photoluminescence to ligand-centered singlet and triplet excited states, consistent within the nature of the dihydrophenazine linker. This assignment is supported by the absence of low-lying metal-centered states in Zn(II), which has a $3d^{10}$ configuration and is thus, photophysically inactive. In Co-HPZDB, the situation is more complex due to the open-shell $3d^7$ high-spin configuration of Co(II). The emission maximum at 850 nm suggests a different origin. Based on the energy and the redox-active nature of the mono-deprotonated $HPZDP^-$ ligand, we consider a metal-to-ligand charge transfer (MLCT) process as a most plausible mechanism—especially because Co(III) in an octahedral coordination with a d^6 low-spin configuration would be very much stabilized. This is supported by prior studies on Co-based coordination compounds showing MLCT-type emissions in the red to near-infrared region.[52,53] While *d*–*d* transitions cannot be fully excluded, their typically spin-forbidden nature in intermediate ligand fields and the concomitant low emission energies lead to longer radiative decay times and thus, make nonradiative relaxation at room temperature a very favorable mechanism. The detection of an emission signal at room temperature despite those challenging conditions may imply a different origin. Furthermore, the emission at long wavelengths

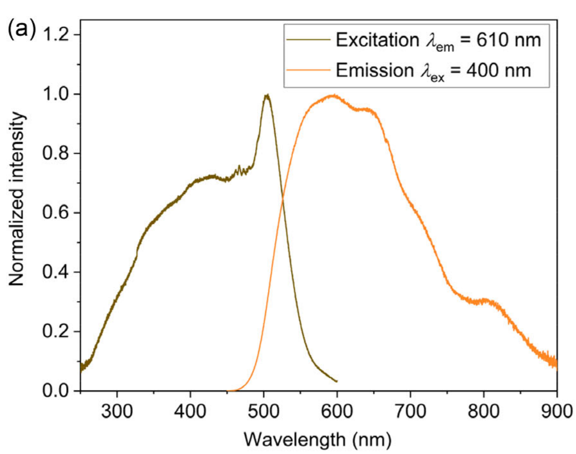

Figure 6. Excitation and emission spectra of powdered a) Zn-PZDB from DEF, and b) Co-HPZDB at room temperature.

compared to the Zn congener is unusual for ligand-centered luminescence alone, additionally supporting a CT-based excited state. Future CASSCF calculations could give more profound insight here.

The thermal stability of Zn-PZDB and Co-HPZDB was investigated by thermogravimetric analysis (TGA) under a nitrogen atmosphere (Figure S11 and S24, Supporting Information). TGA of Zn-PZDB indicates a 30% weight loss at ≈180 °C, which corresponds to the release of two DEF molecules (theoretical 29.4%) with a boiling point of 176–177 °C.[54] The remaining 60% corresponds to PZDB, which does not undergo complete combustion, and metallic Zn (theoretical 61.1%). The residual mass of 10% agrees with the theoretical mass of Zn of 9.5%. For Co-HPZDB, the initial loss of 9.5% corresponds to the loss of one DEF molecule (theoretical 9.1%). The loss of the second DEF overlaps partially with the loss of PZDB, resulting in a combined loss of 83% (theoretical 84.9%). The residual mass of 6% agrees with the theoretical mass of Co of 5.3%.

X-ray photoelectron spectroscopy (XPS) has been performed to investigate the chemical composition and chemical state of Co, N, C, and O in Co-HPZDB. The XPS survey spectrum in the range of binding energies from 0 to 1100 eV in **Figure 7** confirmed the presence of the elements Co, N, C, and O. **Figure 8** shows the high-resolution XPS spectra of C 1*s*, O 1*s*, N 1*s*, Co 2*p*. The high-resolution C 1*s* XPS spectrum exhibits three individual peaks at binding energy values of 284.8, 285.7, and 288.8 eV, which could be assigned to C═C/C─C/C─H, C─N, and O─C═O bonds, respectively corresponding to the arene ring and the carboxylic group in the linker $HPZDB^-$.[55] The high-resolution O 1*s* XPS spectrum is divided into three components, which are composed of oxygen bonded to cobalt (Co─O) and the carboxylic group (O═C─O) of $HPZDB^-$, and absorbed water molecules (─OH) at the binding energy values of 530.8, 531.8, and 532.9 eV, respectively.[56] The N 1*s* high-resolution XPS spectrum shows that in Co-HPZDB, N exists in two chemical states of the phenazine imine (C═N─C) and DEF amide (N─(C═O)─) at the binding energy of 399.0 and 399.7 eV, respectively.[57,58] The Co 2*p* spectrum displayed two main peaks of Co $2p_{3/2}$ (780.6 eV) and Co $2p_{1/2}$ (796.3 eV) with their shake-up satellite peaks (785.6 and 801.2 eV), which can be assigned to Co^{2+} species (Figure 8d).[59]

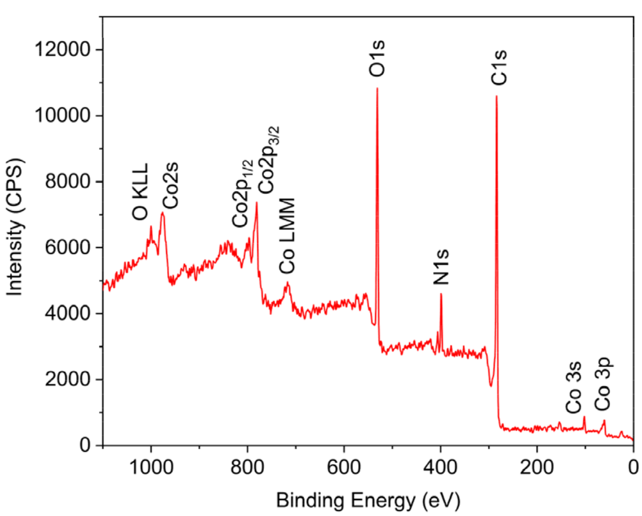

Figure 7. XPS survey spectrum of Co-HPZDB.

2.1. Spectroelectrochemistry of Me_2PZDB and the Coordination Polymers

The typical green coloration observed upon prolonged exposure of the two new CPs to air is highly suggestive of linker oxidation with the concomitant formation of the associated $PZDB^+$ radical cation with an overall charge of −1, considering the deprotonated benzoate groups.[26,50,60] This will likely decrease the binding capabilities of the bridging $PZDB^{2-}$ ligands, thereby opening an avenue for CP degradation. In order to probe experimentally for linker oxidation, we first subjected its dimethyl ester Me_2PZDB to chemical or electrolytic oxidation and measured its UV/Vis/NIR spectrum as a point of comparison with the oxidized samples of Zn-PZDB and Co-HPZDB. Like other 5,10-diaryl-5,10-dihydrophenazines,[25,26,50,51,61–63] Me_2PZDB undergoes two consecutive, chemically and electrochemically reversible one-electron oxidations at half-wave potentials of −130 and 620 mV on the ferrocene/ferrocenium potential scale (Figure S32, Supporting Information). Oxidation past the first anodic peak to the corresponding radical cation inside a spectroelectrochemical cell in the presence of the 1,2-dichloroethane/0.1 mol L^{-1} NBu_4^+ PF_6^- electrolyte caused the growth of new bands at 448 and 475 nm and a vibrationally structured band at lower energy with individual peaks at 572, 629, 685, and 761 nm (Figure S34, Supporting Information). All of these features are typical of 5,10-diphenyl-5,10-dihydrophenazine radical cations;[50,63] they are almost identical to those reported for the closely related *N,N′*-diphenyldihydrophenazine (DPPZ).[63]

In order to monitor the spectroscopic changes accompanying the oxidation of the insoluble Zn-PZDB and Co-HPZDB CPs, we also employed UV/Vis/NIR spectroelectrochemistry. To these ends, an optically transparent ITO electrode was covered with a thin layer of a slurry of the corresponding CP in the ionic liquid 3-butyl-1-methyl-1H-imidazol-3-ium hexafluorophosphate ($BMIM^+$ PF_6^-). The cell was then assembled and filled with an aqueous $NaNO_3$ solution as the electrolyte (for details, see the Experimental Section). On applying a gradually increasing positive potential to the ITO electrode, we observed very similar spectroscopic changes as with dissolved Me_2PZDB (see Figure S34, Supporting Information), that is, the growth of new bands at 443, 470, 623, 681, and 755 nm for Zn-PZDB (**Figure 9**a), or at 443, 472, 630, 687, and 758 nm for Co-HPZDB (Figure S36, Supporting Information). The continuous baseline drift to positive absorbance values during this process hints at the release of the oxidized linker into the ionic liquid. In agreement with this proposition, reduction of the oxidized CPs did not restore the initial state. When subjected to electrolysis under identical conditions, the free H_2PZDB linker provided practically superimposable spectroscopic changes (see the insert of Figure 9a). As a further test for linker oxidation, we subjected dispersions of Zn-PZDP

Research Article
doi.org/10.1002/ejic.202500270

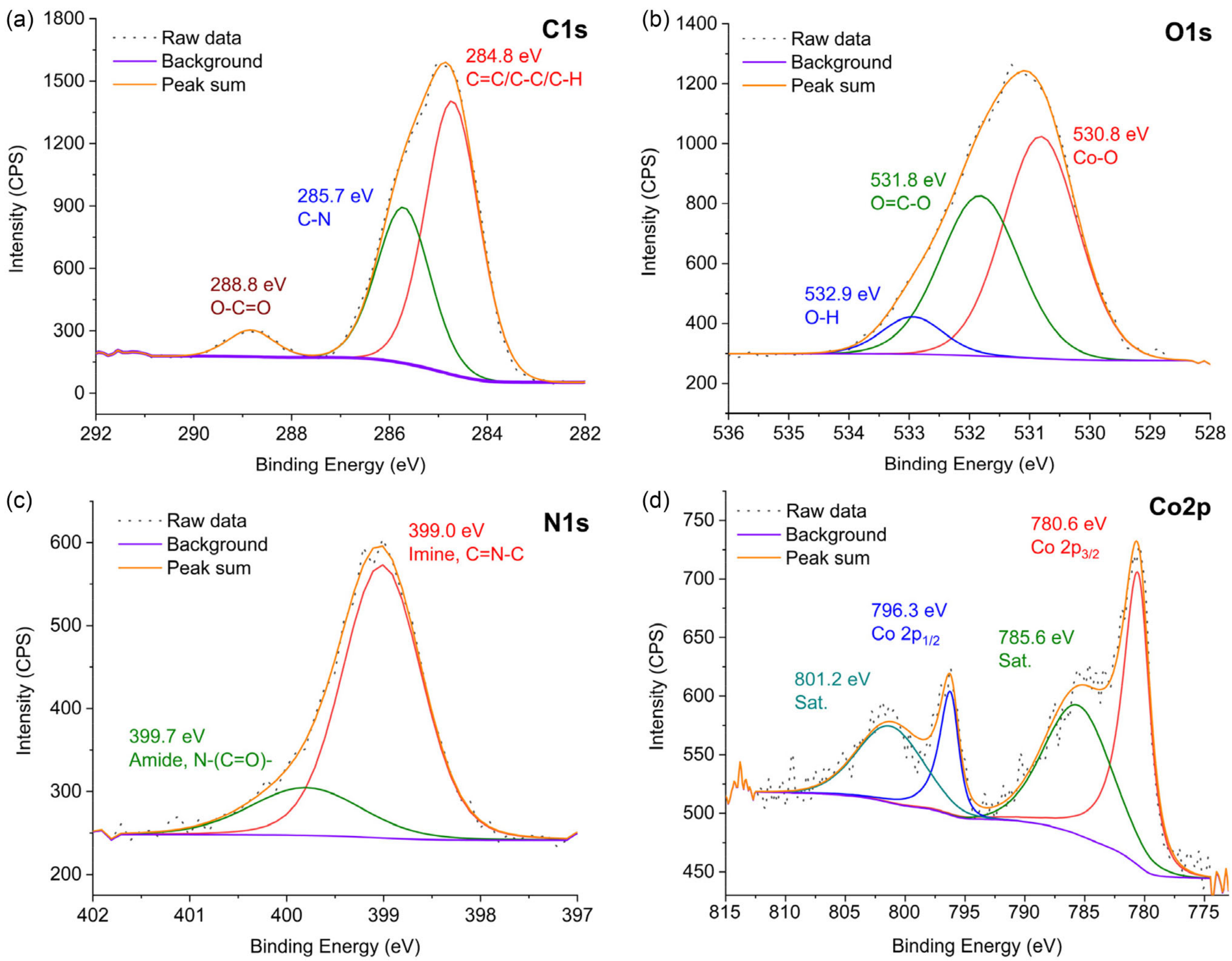

Figure 8. XPS high-resolution spectra of a) C 1*s*, b) O 1*s*, c) N 1*s*, and d) Co 2*p*.

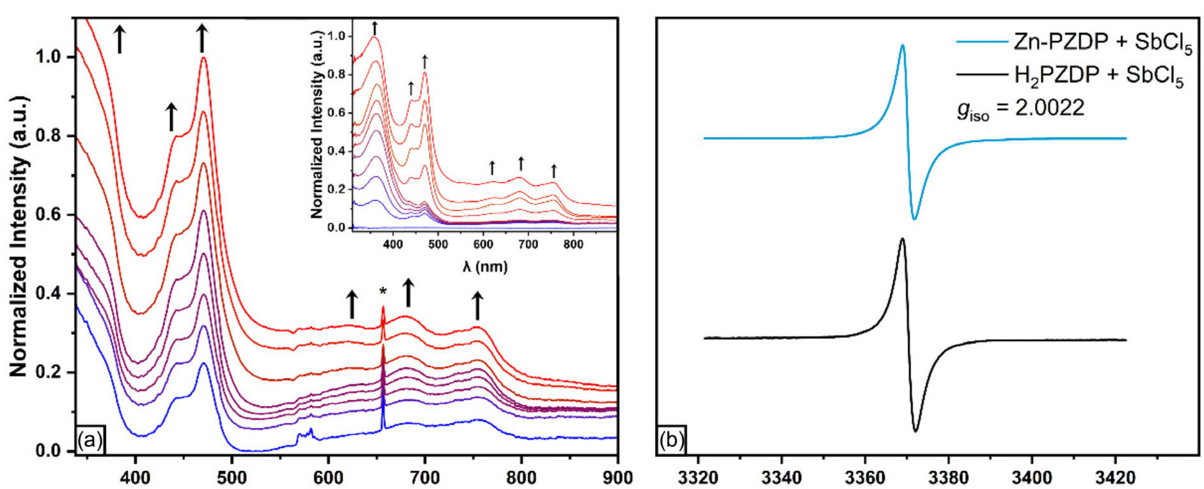

Figure 9. a) UV-Vis spectroelectrochemistry of Zn-PZDB and of H_2PZDB (insert) with oxidation progressing from blue to red lines, measured as pastes in the ionic liquid 3-butyl-1-methyl-1H-imidazol-3-ium hexafluorophosphate ($BMIM^+$ PF_6^-) applied to an ITO-coated glass plate with an aqueous 1 mmol L^{-1} $NaNO_3$ solution as supporting electrolyte at r. t. The asterisk marks an artifact due to the used setup. b) EPR spectra of dispersions of H_2PZDP (black) and Zn-PZDP (blue) in CH_2Cl_2 after addition of sub-stoichiometric amounts of $SbCl_5$ measured with a microwave frequency of 9.404 GHz.

Research Article
doi.org/10.1002/ejic.202500270

(see Figure 9b) (for Co-HPZDB see Figure S36, Supporting Information) and of H_2PZDB in CH_2Cl_2 to oxidation with sub–stoichiometric amounts of $SbCl_5$. In both cases, we observed a rapid color change to a deep blue-green and the concomitant growth of an intense, isotropic EPR resonance signal at a *g*-value of 1.9935, which is typical of the $DPPZ^+$ radical cation (see Figure 9b, right panels).[63]

All these results indicate that the PZDB linker constitutes the primary redox site of these CPs, and that linker oxidation triggers their degradation. This does, however, *per se* not disqualify our new CPs as, for example, photo-redox catalysts, as long as the resulting electron hole is rapidly transferred to a substrate.

3. Conclusion

In summary, this study details the synthesis, structural characterization and redox behavior of two unique coordination polymers (CPs), Zn-PZDB and Co-HPZDB, utilizing the linker acid 4,4′-(phenazine-5,10-diyl)dibenzoic acid (H_2PZDB). The crystallization of H_2PZDB in dimethyl sulfoxide (DMSO) yielded yellow platelets of H_2PZDB·2DMSO in the triclinic space group $P\overline{1}$ (no. 2). Solvothermal reactions of H_2PZDB with Zn(II) or Co(II) nitrate yielded Zn-PZDB and Co-HPZDB. Zn-PZDB crystallizes in monoclinic and triclinic space groups with a **2C1** topology, forming one-dimensional zigzag chains composed of Zn(II) ions coordinated by two monodentate carboxylate ligands and two DEF molecules. The structural details revealed tetrahedral Zn coordination with minor differences in distances and angles between the monoclinic and triclinic forms. Co-HPZDB crystallizes in the orthorhombic space group *Ccce* (no. 68) with a sql topology, forming two-dimensional layers with disordered octahedral cobalt coordination. Each Co(II) ion is coordinated by two DEF molecules and two $HPZDB^-$ linkers, with hydrogen bonding and stacking interactions extending to a three-dimensional supramolecular structure. Upon exposure to air, the CPs exhibit a green coloration, indicative of the oxidation of the (H)$PZDB^{-/2-}$ linkers, which lead to the degradation of the CPs. UV/Vis/NIR spectroelectrochemical studies of Me_2PZDB showed two reversible one-electron oxidations, producing characteristic absorbance bands. Similar spectroscopic changes were observed for Zn-PZDB and Co-HPZDB upon oxidation, indicating the presence of oxidized linker. Chemical oxidation with $SbCl_5$ was employed to confirm the formation of (H)$PZDB^{0/-}$ radicals, evidenced by a rapid color change and isotropic EPR resonance signals. The findings indicate that the (H)PZDB linker is the primary redox site, and its oxidation triggers CP degradation. However, this redox activity does not necessarily disqualify the CPs from applications such as photo-redox catalysis, provided that the resulting electron hole can be efficiently transferred to a substrate. Thus, the study does not only provide a comprehensive synthesis and characterization of the CPs, but also highlights their potential utility in catalytic applications despite the challenges posed by linker oxidation.

4. Experimental Section

All chemicals were commercially obtained and used without further purification (see ESI, Section S1 for details of commercial suppliers). The water used was deionized.

Fourier-transform infrared (FT-IR) spectra were recorded on a Bruker FT-IR Tensor 37 spectrometer in the attenuated total reflection (ATR) mode in the range of 4000–550 cm^{-1}.

Thermogravimetric analyses (TGA) were performed on a Netzsch Tarsus TG 209 instrument under nitrogen from room temperature to 1000 °C with a heating rate of 5 °C min^{-1} in Al_2O_3 crucibles.

NMR spectra were obtained on a Bruker Avance III-300 (Bruker, Billerica, MA, USA) (^{1}H: 300 MHz); ^{13}C{^{1}H}: 75 MHz) in $CDCl_3$, C_6D_6 and DMSO-d_6. The spectra were referenced on the residual solvent peak (^{1}H NMR $\delta = 7.26$ ppm for $CDCl_3$, 7.16 ppm for C_6D_6 and 2.50 ppm for DMSO-d_6).

Elemental analyses were performed using an Elementar Vario MICRO Cube analyzer. Due to technical limitations, it was not possible to shield the samples from ambient air and moisture during weighing and handling, leading to deviations.

X-ray photoelectron spectroscopy (XPS) was carried out using a ULVAC-PHI VersaProbe II microfocus spectrometer equipped with an Al Kα X-ray source (1486.8 eV). The spectra were analyzed with the Casa XPS software, version 2.3.19PR1.0 from Casa Software Ltd, Teignmouth, UK.

Powder X-ray diffraction (PXRD) measurements were performed at room temperature using a Rigaku Miniflex 600 powder diffractometer (Rigaku, Tokyo, Japan) with Cu Kα1 radiation ($\lambda = 1.5406$ Å, 40 kV, 15 mA, 600 W) covering a 2θ range of 2°–50°. The analysis utilized a flat silicon low-background holder with a small indent for placing the sample.

Solid-state luminescence measurements were carried out using an FLS1000 photoluminescence spectrometer from Edinburgh Instruments. The system featured a 450 W Xe arc lamp as the excitation source, double grating monochromators in Czerny-Turner configuration in both the excitation and emission compartment, and a thermoelectrically cooled photomultiplier tube (PMT-980) from Hamamatsu, maintained at −20 °C. Emission spectra were corrected for both grating efficiency and PMT sensitivity, while excitation spectra were additionally corrected to account for fluctuations of the lamp intensity. Time-resolved photoluminescence was recorded using pulsed laser diodes EPL-450 (Edinburgh Instruments, temporal pulse width: 90 ps, 0.15 mW average incident peak power) or VPL-450 (Edinburgh Instruments, operating at 90 mW average incident peak power in continuous-wave mode) with adjustable pulse widths (0.1–1 ms) and variable trigger frequencies (0.1 Hz to 5 MHz). Time-correlated single photon counting (TCSPC) was employed as the detection mode for time-resolved measurements.

For single-crystal X-ray diffraction suitable crystals were selected with care under a polarized-light microscope, coated with protective oil, and mounted on a cryo-loop. The data were acquired using a Rigaku XtaLAB Synergy diffractometer equipped with a Hybrid Pixel Array Detector and a microfocus sealed X-ray tube PhotonJet (Cu) X-ray source ($\lambda = 1.54184$ Å). Cell refinement, data reduction, and absorption correction were performed using CRYSALISPRO. The structure was determined with SHELXT and further refined with SHELXL, utilizing OLEX2 as the interface. Figures were generated using the DIAMOND 4.0 software. Additional crystal data can be found in the Supporting Information.

Deposition Numbers 2 453 691 (for H_2PZDB·2DMSO), 2 453 692 (for Zn-PZDB, 150 K), 2 453 693 (for Zn-PZDB, 298 K), 2 453 694 (for Zn-PZDB with DMF), 2 453 695 (for Co-HPZDB, non-disordered), 2 453 696 (for Co-HPZDB, disordered) contain the supplementary crystallographic data for this article. These data are provided free of charge by the joint Cambridge Crystallographic Data Center and Fachinformationszentrum Karlsruhe Access Structures service.[64]

Cyclic voltammetry of Me_2PZDP was conducted under an argon atmosphere. The voltammograms were recorded using a BASi Epsilon potentiostat and a custom-built cell as previously described.[65] A platinum working electrode (∅ = 1.1 mm, BASi) was used. The platinum electrode was polished before each measurement series with diamond pastes from Buehler & Wirtz (grain sizes 1 and 0.25 μm). Spiral-shaped AgCl and Pt wires were used as the reference and counter electrode. The supporting electrolyte was a 0.1 mol L^{-1} solution of nBu_4N^+ PF_6^- in CH_2Cl_2. The redox potentials were referenced against the FcH/FcH^+ redox couple ($E_{1/2}$ = 0.000 V).

UV-Vis/NIR spectroscopy and spectroelectrochemical measurements were acquired with a TIDAS fiber optic diode array spectrometer, which consists of a combination of MCS UV/NIR and PGS NIR instruments from j&m Analytik AG. For the determination of the extinction coefficients, a quartz cell with an optical path length of 0.2 cm was used. A Wenking Pos 2 potentiostat from intelligent controls GmbH was used for spectroelectrochemical measurements on dissolved samples in combination with a custom-made optically transparent electrochemical thin-layer cell (OTTLE) according to Hartl's design.[66] The OTTLE cell consists of a working and counter electrode made of Pt grids and a thin silver wire as a pseudo reference electrode, sandwiched in between two optically transparent CaF_2 windows. 1,2-$C_2H_4Cl_2$ was used as the solvent with 0.1 mol L^{-1} nBu_4N^+ PF_6^- as the supporting electrolyte. Spectroelectrochemical measurements of insoluble Zn-PZDP, Co-HPZDP, and H_2PZDP were recorded as pastes of the analyte with the ionic liquid $BMIM^+$ PF_6^-, applied on an ITO-coated, electrically conductive transparent plate as the working electrode. The latter was assembled in a Teflon cell together with a platinum and Ag/AgCl wire as counter and pseudo reference electrode, respectively. An aqueous $NaNO_3$ solution (1 mmol L^{-1}) was used as supporting electrolyte. The potential was applied using a BASi Epsilon potentiostat, and the UV/Vis spectra were continuously recorded upon applying a potential sweep at a scan rate of 2 mV s^{-1}. Both CPs were generally oxidized under inert atmosphere (except for the control experiment in Figure S36, Supporting Information). The paste with the ionic liquid had to be prepared under ambient atmosphere. After assembling the cell, we flushed the setup with argon, as to be able to conduct the spectroelectrochemical measurement under inert gas atmosphere, and in the absence of oxygen. Based on the initial UV-Vis absorption spectrum we can confirm the fully reduced sample was present at the start of the experiment.

EPR spectra were recorded under inert atmosphere using a X-band tabletop spectrometer MiniScope MS 400 by Magnettech GmbH.

Synthesis

5,10-Dihydrophenazine: Phenazine (5.0 g, 27.7 mmol) was dissolved in ethanol (125 mL), sodium dithionite (48.2 g, 277 mmol) in de-ionized water (500 mL), and both solutions were combined and heated under stirring and reflux for 3 h or overnight. The precipitate was filtered off and washed three times with deionized water. Finally, the solid was dried at 20 °C in vacuum (1×10^{-3} mbar) for 16 h. The product (yield 4.75 g, 94%) was obtained as a light green solid and was used without further purification. Important: The dihydrophenazine solid must be stored under a protective gas atmosphere (nitrogen or argon), otherwise it re-oxidizes which is evidenced by a gradual color change to dark blue and then black. [^{1}H NMR] (600 MHz, $CDCl_3$) δ (ppm) = 8.27 (dd, J = 6.8, 3.5 Hz, 1 H), 7.86 (dd, J = 6.8, 3.4 Hz, 1 H), 6.12 (s, 2 H).

Dimethyl-4,4′-(phenazine-5,10-diyl)dibenzoate (Me_2PZDB): 5,10-Dihydrophenazine (1.0 g, 5.49 mmol), methyl-4-bromobenzoate (2.6 g, 12.1 mmol) and anhydrous potassium carbonate (1.52 g, 11.0 mmol) were dissolved in degassed xylene (25 mL). Palladium (II) acetate (62 mg, 5 mol%) and tri-*tert*-butylphosphine (111 mg, 10 mol%) were dissolved in degassed xylene (25 mL). Both solutions were combined under stirring. Under nitrogen inert gas the reaction mixture was heated under stirring to reflux for 48 h. After cooling to room temperature, water (100 mL) was added to the reaction mixture and the water/xylene mixture was extracted three times with dichloromethane (3 × 150 mL). The organic phases were combined and dried over magnesium sulfate (30 min). All solvents were removed using a rotary evaporator. The crude product was washed three times with ethanol (100 mL). The product was finally filtered and dried in vacuo at 60 °C for 16 h (yield 2.25 g, 91%). [^{1}H NMR] (300 MHz, C_6D_6) δ/ppm = 8.11 (d, J = 8.4 Hz, 4 H), 7.06 (d, J = 8.5 Hz, 4 H), 6.35 (dd, J = 5.9, 3.4 Hz, 4 H), 5.81 (dd, J = 5.9, 3.4 Hz, 4 H), 3.52 (s, 6 H). [^{13}C NMR] (75 MHz, C_6D_6) δ (ppm) = 166.0, 145.2, 136.6, 132.9, 131.0, 130.1, 122.0, 113.9, 52.5. [HR-ESI-MS] m/z = 450.1582 (calculated for $^{12}C_{28}$ $^{1}H_{22}$ $^{14}N_2$ $^{16}O_4$ 450.1580). [IR] (ATR) v (cm^{-1}) = 2955 (m), 1723 (s), 1590 (m), 1483 (s), 1344 (s), 1285 (s), 1265 (s), 1110 (w), 1095 (w), 724 (w), 701 (w). [EA] Calc. for $C_{28}H_{22}N_2O_4$: C 74.65, H 4.92, N 6.22 – found: C 74.78, H 4.93, N 6.11%. [M.p] 296 °C.

4,4′-(Phenazine-5,10-diyl)dibenzoic acid (H_2PZDB): Dimethyl-4,4′-(phenazine-5,10-diyl)dibenzoate (450.5 mg, 1.0 mmol) was dissolved in 1,4-dioxane (30 mL). Lithium hydroxide (419.6 mg, 10.0 mmol) was dissolved separately in 15 mL of water and added to the reaction mixture, which was then heated overnight under reflux (100 °C). With the assistance of a pipette, hydrochloric acid was carefully added the following day until a pH value of ≈1–2 was reached. Afterwards, 100 mL of water were added to the mixture and stirred for another 3 h. The formed yellow precipitate was filtered off and washed with water. Finally, the orange solid obtained was dried in vacuo at 60 °C for 16 h (yield 0.372 g, 88%). Single crystals suitable for X-ray crystallography were grown from a saturated DMSO solution. [^{1}H NMR] (300 MHz, DMSO-d_6) δ (ppm) = 8.20 (d, J = 8.4 Hz, 4 H), 7.54 (d, J = 8.4 Hz, 4 H), 6.37 (dd, J = 5.9, 3.4 Hz, 4 H), 5.67 (dd, J = 5.9, 3.4 Hz, 4 H). [^{13}C NMR] (75 MHz, DMSO-d_6) δ (ppm) = 166.7, 144.1, 135.6, 132.5, 130.6, 130.5, 121.5, 113.2. [HR-ESI-MS] m/z = 422.1269 (calculated for $^{12}C_{26}$ $^{1}H_{18}$ $^{14}N_2$ $^{16}O_4$ 422.1267). [IR] (ATR) v (cm^{-1}) = 3454 (m), 1692 (s), 1656 (m), 1593 (m), 1484 (s), 1418 (w), 1346 (s), 1280 (s), 1119 (w), 1091 (w), 735 (w). [EA] Calc. for $C_{26}H_{18}N_2O_4$: C 73.92, H 4.30, N 6.63 – found: C 73.10, H 4.36, N 6.42%. [M.p] > 350 °C.

Zn-PZDB: Zinc nitrate hexahydrate (800 mg, 2.69 mmol) and 4,4′-(phenazine-5,10-diyl)dibenzoic acid (100 mg, 0.24 mmol) were added to 10 mL of DEF in a Pyrex tube (20 mL). The reaction mixture was then placed in an ultrasonic bath at 40 °C for ≈30 min until a homogeneous solution was obtained. The reaction was carried out for 72 h at 85 °C (plus 3 h heating/3 h cooling) in a programmable synthesis oven. Subsequently, the crude product was washed three times with DEF (5 mL each). The crystalline MOF was finally dried by high vacuum (1×10^{-3} mbar) for 16 h and stored under inert gas atmosphere. The final product was obtained as clear yellow crystals. Yield: 26.0%, 42.8 mg, [EA] Calc. for $C_{36}H_{38}N_4O_6Zn$: C 62.84, H 5.57, N 8.14 – found: C 62.23, H 5.38, N 8.16%. [IR] (ATR) v (cm^{-1}) = 2978 (w), 2919 (w), 2881 (w), 1573 (s), 1482 (m), 1401 (m), 1331 (s), 1281 (m), 1264 (m), 1088 (w), 1061 (w), 781 (m), 731 (m), 707 (w), 667 (w).

Co-HPZDB: Cobalt nitrate hexahydrate (800 mg, 2.75 mmol), lithium chloride (10 mg, 0.24 mmol) and 4,4′-(phenazine-5,10-diyl)dibenzoic acid (100 mg, 0.24 mmol) were added to 10 mL of DEF in a Pyrex tube (20 mL). The reaction mixture was then placed in an ultrasonic bath at 40 °C for ≈30 min until a homogeneous solution was obtained. The reaction was carried out for 72 h at 85 °C (3 h heating/3 h cooling) in a programmable synthesis oven. Subsequently, the crude product was washed three times with DEF (5 mL). The crystalline MOF was finally dried in high vacuum (1×10^{-3} mbar) for 16 h and stored under inert gas atmosphere. The product was obtained as a dark brown/purple crystalline solid. Yield: 11.8%, 31.5 mg. [EA] Calc. for $C_{62}H_{54}CoN_6O_{10}$: C 67.14, H 4.91, N 7.58 – found: C 67.32, H 5.12, N 7.55%. [IR] (ATR) v

(cm^{-1}) = 3048 (w), 2985 (w), 2946 (w), 2910 (w), 2880 (w), 1639 (s), 1591 (s), 1483 (s), 1456 (m), 1386 (m), 1346 (m), 1284 (m), 1265 (m), 1215 (w), 1160 (w), 1092 (w), 1059 (w), 824 (m), 780 (m), 733 (s), 707 (m), 659 (m), 616 (w).

Supporting Information

The authors have cited additional references within the Supporting Information.[67–74]

Acknowledgements

The authors thank Dr. István Boldog for the project proposal, supervision during initial stages of the work, and crystallographic support. D.P. and C.J. thank the Deutsche Forschungsgemeinschaft (DFG, German Research Foundation) for grant 396890929/GRK 2482. The Rigaku X-ray diffractometer was funded by the DFG through grant 440366605. M.S. gratefully acknowledges funding from a materials cost allowance of the Fonds der Chemischen Industrie e.V. and a scholarship from the "Young College" of the North-Rhine Westphalian Academy of Sciences and Arts. The authors thank T.S. for the measurements of the thermogravimetric analysis. The authors thank Birgit Tommes for the IR measurements and Annette Ricken for the AAS measurements. The authors also thank the Center for Molecular and Structural Analytics at Heinrich Heine University (CeMSA@HHU) for recording the mass spectrometric and NMR-spectrometric data.

Conflict of Interest

The authors declare no conflict of interest.

Data Availability Statement

The data that support the findings of this study are available in the supplementary material of this article.

Keywords: coordination polymers · dihydrophenazine · radical cation · redox-active linker · spectroelectrochemistry

[1] S. R. Batten, N. R. Champness, X.-M. Chen, J. Garcia-Martinez, S. Kitagawa, L. Öhrström, M. O'Keeffe, M. P. Suh, J. Reedijk, *Pure Appl. Chem.* **2013**, *85*, 1715.
[2] G. H. Morritt, H. Michaels, M. Freitag, *Chem. Phys. Rev.* **2022**, *3*, 011306.
[3] C. Janiak, J. K. Vieth, *New J. Chem.* **2010**, *34*, 2366.
[4] N. Stock, S. Biswas, *Chem. Rev.* **2012**, *112*, 933.
[5] L. Chen, X. Zhang, X. Cheng, Z. Xie, Q. Kuang, L. Zhenga, *Nanoscale Adv.* **2020**, *2*, 2628.
[6] S. Mohadeseh, F. M. Mehdi, E. Nasser, J. Shohreh, O. Ali, K. Mehrdad, *Trends Anal. Chem.* **2019**, *118*, 401.
[7] G. I. Dzhardimalieva, I. E. Uflyand, *RSC Adv.* **2017**, *7*, 42242.
[8] S. R. Batten, B. Chen, J. J. Vittal, *ChemPlusChem* **2016**, *81*, 669.
[9] K. Biradha, A. Goswami, R. Moi, *Chem. Commun.* **2020**, *56*, 10824.
[10] S. Chorazy, M. Wyczesany, B. Sieklucka, *Molecules* **2017**, *22*, 1902.
[11] X. Liu, S. Wang, W. Xie, J. Ni, K. Xiao, S. Liu, W. Lv, Q. Zhao, *J. Mater. Chem. C* **2023**, *11*, 7405.
[12] *Introduction to Reticular Chemistry. Metal-Organic Frameworks and Covalent Organic Frameworks* (Eds: O. M. Yaghi, M. J. Kalmutzki, C. S. Diercks), Wiley-VCH Verlag GmbH & Co. KGaA, Weinheim **2019**.
[13] B. Ding, M. B. Solomon, C. F. Leong, D. M. D'Alessandro, *Coord. Chem. Rev.* **2021**, *439*, 213891.
[14] D. M. D'Alessandro, *Chem. Commun.* **2016**, *52*, 8957.
[15] P.-Q. Liao, J.-Q. Shen, J.-P. Zhang, *Coord. Chem. Rev.* **2018**, *373*, 22.
[16] J.-K. Sun, L.-X. Cai, Y.-J. Chen, Z.-H. Li, J. Zhang, *Chem. Commun.* **2011**, *47*, 6870.
[17] M. Higuchi, K. Nakamura, S. Horike, Y. Hijikata, N. Yanai, T. Fukushima, J. Kim, K. Kato, M. Takata, D. Watanabe, S. Oshima, S. Kitagawa, *Angew. Chem. Int. Ed.* **2012**, *51*, 8369.
[18] C. Krämer, U. Wild, O. Hübner, C. Neuhäuser, E. Kaifer, H.-J. Himmel, *Aust. J. Chem.* **2014**, *67*, 1044.
[19] U. Wild, E. Kaifer, H. Wadepohl, H.-J. Himmel, *Eur. J. Inorg. Chem.* **2015**, *2015*, 4848.
[20] Y.-G. Weng, Z.-H. Ren, Z.-R. Zhang, J. Shao, Q.-Y. Zhu, J. Dai, *Inorg. Chem.* **2021**, *60*, 17074.
[21] H.-Y. Wang, L. Cui, J.-Z. Xie, C. F. Leong, D. M. D'Alessandro, J.-L. Zuo, *Coord. Chem. Rev.* **2017**, *345*, 342.
[22] F. Solano, P. Auban-Senzier, I. Olejniczak, B. Barszcz, T. Runka, P. Alemany, E. Canadell, N. Avarvari, N. Zigon, *Chem. Eur. J.* **2023**, *29*, e202203138.
[23] F. Manna, M. Oggianu, P. Auban-Senzier, G. Novitchi, E. Canadell, M. L. Mercuri, N. Avarvari, *Chem. Sci.* **2024**, *15*, 19247.
[24] J. Lee, K. Shizu, H. Tanaka, H. Nakanotani, T. Yasuda, H. Kaji, C. Adachi, *J. Mater. Chem. C* **2015**, *3*, 2175.
[25] D. A. Corbin, B. G. McCarthy, Z. van de Lindt, G. M. Miyake, *Macromolecules* **2021**, *54*, 4726.
[26] S. Suzuki, T. Takeda, M. Kuratsu, M. Kozaki, K. Sato, D. Shiomi, T. Takui, K. Okada, *Org. Lett.* **2009**, *11*, 2816.
[27] F. Unglaube, P. Hünemörder, X. Guo, Z. Chen, D. Wang, E. Mejía, *Helv. Chim. Acta* **2020**, *103*, e2000184.
[28] J. Lin, J. Ouyang, T. Liu, F. Li, H. H.-Y. Sung, I. Williams, Y. Quan, *Nat. Commun.* **2023**, *14*, 7757.
[29] Q.-Y. Hong, B. Huang, M.-X. Wu, L. Xu, X.-L. Zhao, X. Shi, H.-B. Yang, *Chin. J. Chem.* **2024**, *42*, 1895.
[30] J. C. Theriot, C.-H. Lim, H. Yang, M. D. Ryan, C. B. Musgrave, G. M. Miyake, *Science* **2016**, *352*, 1082.
[31] K. Wang, X. Kang, C. Yuan, X. Han, Y. Liu, Y. Cui, *Angew. Chem. Int. Ed.* **2021**, *60*, 19466.
[32] W. L. Jiang, B. Huang, X. L. Zhao, X. Shi, H. B. Yang, *Chem* **2023**, *9*, 2655.
[33] I. Kochetygov, J. Roth, J. Espín, S. Pache, A. Justin, T. Schertenleib, N. Taheri, D. Chernyshov, W. L. Queen, *Angew. Chem. Int. Ed.* **2023**, *62*, e202215595.
[34] W.-L. Jiang, B. Huang, M.-X. Wu, Y.-K. Zhu, X.-L. Zhao, X. Shi, H.-B. Yang, *Chem. Asian J.* **2021**, *16*, 3985.
[35] M.-X. Wu, Q.-Y. Hong, M. Li, W.-L. Jiang, B. Huang, S. Lu, H. Wang, H.-B. Yang, X.-L. Zhao, X. Shi, *Chem. Commun.* **2024**, *60*, 1184.
[36] H. Zhang, X. Tanga, C. Gu, *J. Mater. Chem. A* **2021**, *9*, 4984.
[37] Y. Cheng, Y.-X. Li, C.-H. Liu, Y.-Y. Zhu, W. Lin, *Angew. Chem. Int. Ed.* **2023**, *62*, e202310470.
[38] S. Xu, H. Dai, S. Zhu, Y. Wu, M. Sun, Y. Chen, K. Fan, C. Zhang, C. Wang, W. Hu, *eScience* **2021**, *1*, 60.
[39] F. A. Obrezkov, V. Ramezankhani, I. Zhidkov, V. F. Traven, E. Z. Kurmaev, K. J. Stevenson, P. A. Troshin, *J. Phys. Chem. Lett.* **2019**, *10*, 5440.
[40] M.-X. Wu, Y. Li, J. Liu, B. Huang, Q.-Y. Hong, W.-L. Jiang, Y. Zhao, G. Dai, B. Hu, X. Shi, H.-B. Yang, *Angew. Chem. Int. Ed.* **2025**, *64*, e202503151.
[41] Q. Wang, X. Wang, Y. Zhai, Z. Zheng, H. Shen, Y. Han, Z. Chen, Z. Jiang, *Molecules* **2024**, *29*, 1618.
[42] G. Dai, Y. He, Z. Niu, P. He, C. Zhang, Y. Zhao, X. Zhang, H. Zhou, *Angew. Chem. Int. Ed.* **2019**, *58*, 9902.
[43] D. Püschel, J. Wiefermann, S. Hédé, T. Heinen, L. Pfeifer, O. Weingart, M. Suta, T. J. J. Müller, C. Janiak, *J. Mater. Chem. C* **2023**, *11*, 8982.
[44] A. P. Shevchenko, A. A. Shabalin, I. Y. Karpukhin, V. A. Blatov, *Sci. Technol. Adv. Mater.* **2022**, *2*, 250.
[45] S. J. Bora, M. Chakrabortty, B. K. Das, *J. Mol. Struct.* **2020**, *1217*, 128434.
[46] F. Dimakopoulou, C. G. Efthymiou, A. Kourtellaris, C. O'Malley, L. A. E. Refat, A. Tasiopoulos, P. McArdle, C. Papatriantafyllopoulou, *CrystEngComm* **2023**, *25*, 6080.
[47] J.-G. Wang, J.-H. Qin, L. Li, L.-F. Ma, *Synth. React. Inorg., Met.-Org., Nano-Met. Chem.* **2014**, *44*, 112.

[48] L.-L. Kong, S. Gao, L.-H. Huo, *Acta Cryst.* **2007**, *E63*, m2554.
[49] J.-W. Lei, C.-X. Xie, H.-X. Yang, *Acta Cryst.* **2012**, *E68*, m697.
[50] G. Xie, N. M. Bojanowski, V. Brosius, T. Wiesner, F. Rominger, J. Freudenberg, U. H. F. Bunz, *Chem. Eur. J.* **2021**, *27*, 1976.
[51] K. Yazaki, S. Noda, Y. Tanaka, Y. Sei, M. Akita, M. Yoshizawa, *Angew. Chem. Int. Ed.* **2016**, *55*, 15031.
[52] N. Sinha, B. Pfund, C. Wegeberg, A. Prescimone, O. S. Wenger, *J. Am. Chem. Soc.* **2022**, *144*, 9859.
[53] J. Jin, Y. Gong, L. Li, X. Han, Q. Meng, Y. Liu, S. Niu, *Spectrochim. Acta A* **2015**, *137*, 856.
[54] Entry for *N,N*-diethylformamide in the *GESTIS-Stoffdatenbank* of the IFA, https://gestis.dguv.de/data?name=012220, retrieved on the 12th April **2024**.
[55] M. C. Biesinger, *Appl. Surf. Sci.* **2022**, *597*, 153681.
[56] P. Luo, S. Li, Y. Zhao, G. Ye, C. Wei, Y. Hu, C. Wei, *ChemCatChem* **2019**, *11*, 6061.
[57] C. D. Wagner, A. V. Naumkin, A. Kraut-Vass, J. W. Allison, C. J. Powell, J. R. Jr. Rumble, NIST Standard Reference Database 20, Version 3.4 (web version), **2003**. (http://srdata.nist.gov/xps/).
[58] A. Mohtasebi, T. Chowdhury, L.-H. Hsu, M. C. Biesinger, P. Kruse, *J. Phys. Chem. C* **2016**, *120*, 29248.
[59] M. C. Biesinger, B. P. Payne, A. P. Grosvenor, L. W. Lau, A. R. Gerson, R. S. C. Smart, *Pure Appl. Chem.* **2011**, *257*, 2717.
[60] S. Suzuki, D. Yamaguchi, Y. Uchida, T. Naota, *Angew. Chem. Int. Ed.* **2021**, *60*, 8284.
[61] M. Schorpp, T. Heizmann, M. Schmucker, S. Rein, S. Weber, I. Krossing, *Angew. Chem. Int. Ed.* **2020**, *59*, 9453.
[62] J. P. Cole, C. R. Federico, C.-H. Lim, G. M. Miyake, *Macromolecules* **2019**, *52*, 747.
[63] B. Huang, H. Kang, X.-L. Zhao, H.-B. Yang, X. Shi, *Cryst. Growth Des.* **2022**, *22*, 3587.
[64] Deposition numbers 2453691 (for H_2PZDB·2DMSO), 2453692 (for Zn-PZDB, 150 K), 2453693 (for Zn-PZDB, 298 K), 2453694 (for Zn-PZDB, with DMF), 2453695 (for Co-HPZDB, non-disordered), and 2453696 (for Co-HPZDB, disordered) contain the supplementary crystallographic data for this paper. These data are provided free of charge at www.ccdc.cam.ac.uk/data_request/cif.
[65] N. Rotthowe, J. Zwicker, R. F. Winter, *Organometallics* **2019**, *38*, 2782.
[66] M. Krejčik, M. Daněk, F. Hartl, *J. Electroanal. Chem.* **1991**, *317*, 179.
[67] A. L. Spek, *Acta Crystallogr. D* **2009**, *65*, 148.
[68] A. L. Spek, *PLATON – A Multipurpose Crystallographic Tool*, Utrecht University, Utrecht, The Netherlands **2005**.
[69] M. Nishio, *Phys. Chem. Chem. Phys.* **2011**, *13*, 13873.
[70] M. Nishio, Y. Umezawa, K. Honda, S. Tsuboyama, H. Suezawa, *CrystEngComm* **2009**, *11*, 1757.
[71] M. Nishio, *CrystEngComm* **2004**, *6*, 130.
[72] C. Janiak, S. Temizdemir, S. Dechert, W. Deck, F. Girgsdies, J. Heinze, M. J. Kolm, T. G. Scharmann, O. M. Zipffel, *Eur. J. Inorg. Chem.* **2000**, *2000*, 1229.
[73] Y. Umezawa, S. Tsuboyama, K. Honda, J. Uzawa, M. Nishio, *Bull. Chem. Soc. Jpn.* **1998**, *71*, 1207.
[74] M. Nishio, M. Hirota, Y. Umezawa, *The CH/π; Interaction: Evidence, Nature, and Consequences*, Wiley-VCH, New York, Germany **1998**, https://www.wiley.com/en-us/The+CH+%26pi%3B+Interaction%3A+Evidence%2C+Nature%2C+and+Consequences-p-9780471252900.

Manuscript received: May 26, 2025
Revised manuscript received: July 7, 2025
Version of record online: August 19, 2025